NUMERICAL ANALYSIS OF FLOW MECHANISM BETWEEN SEALING FLOW AND MAINSTREAM EXHAUSTED FROM PULSE DETONATION COMBUSTOR

Bo WANG, Long-Xi ZHENG, Jie LU [*], Yu-Dong YANG, Dao-En ZHOU

School of Power and Energy, Northwestern Polytechnical University, Xi'an 710072, China

[*] Corresponding author; E-mail: lujie@nwpu.edu.cn

A conventional axial turbine drived by a pulse detonation combustor heavily challenges the turbine cooling and hot gas sealing. In order to fully understand the physical behavior of ingress and egress effect with the pulse inlet mainstream, a study is carried out to investigate the unsteady flow field and sealing efficiency inside the cavity using the method of unsteady, three-dimensional Computational Fluid Dynamic simulation. The pulse detonation inflow boundary condition simplified using simple exponential decay formulas are applied to the inlet of mainstream passage. The results reveal that the magnitude of sealing gas pressure does affect the pressure and sealing efficiency distribution inside cavity. The sealing efficiency inside the cavity goes through three sub-stages, respectively, " the decline stage", " the plateau stage " and " the recovery stage ". when the sealing gas pressure increases, the sealing efficiency of these three sub-stages will increase, and the duration of " the plateau stage " and " the recovery stage " will decrease. As a result, the ability of turbine cavity that resist the ingress of pulse detonation inflow can be augmented with the sealing gas pressure increases.

Key words*: numerical simulation, pulse detonation combustion, turbine cavity, pressure coefficient, sealing efficiency*

1. Introduction

The increasing demand to reduce specific fuel consumption within the current turbofan engines in recent years results in the studies of the Pulse detonation turbine engine (PDTE), which is based on detonation instead of the deflagration currently used in conventional combustion chamber. One reason for this seems to be the basic pulse detonation cycle is thermodynamically similar to the constant volume combustion. The achievable ideal thermal efficiency of pulse detonation engine has been estimated up to 80% by Heiser and Pratt [1]. However, lots of challenges arise as a result of pulse detonation combustion is highly transient and complex. The turbine component has to work with unsteady, pulse inlet flow, which could affect the performance of turbine cooling and hot gas sealing. Current conventional turbines use the gas generally bled from compressor as cooling gas to prevent the hot mainstream gas ingress into the cavity between the stationary and rotating disc. The sealing concept of conventional turbines might not applicable to the cavity of PDTE due to the total pressure in the inlet of turbine is higher than that in the compressor. Therefore, there is a significant need for designing innovative sealing concepts and suitable rim seal structures for PDTE. There have been lots of investigations into the rim seal in the last decade years.

R.P.Roy et al. [2] carried out a study that combine experiments in a model single-stage axial turbine with computational fluid dynamic simulations. The unsteady, three-dimensional CFD simulation corroborated the interpretation that the high tangential velocity fluid is comprised of the ingested main air, while the lower tangential velocity fluid is the indigenous cavity air. D.W.Zhou et al. [3] exported the measurement of the time-average but spatially local main gas ingestion and the instantaneous velocity field in the rim cavity. Roy Teuber et al. [4] used unsteady Reynolds-averaged Navier-Stokes computations to study the fluid mechanics of two different rim seal geometries based on an experimental test rig at the University of Bath. They compared a certain range of sealing flow rates and found that the minimum sealing flow rate required to prevent ingestion increased as mainstream Mach number increases. T.Schliwka et al. [5] examined the impact of an unsteady combustion to the turbine sealing cavity through the experiments carried out at the Hot-Acoustic-Test Rig (HAT) wind tunnel at the TU Berlin. The unsteady flow measured by pressure tabs with high time resolution showed the total pressure loss inside the vane wake. Jun Li et al. [6] numerically compared the sealing performance between conventional radial rim seal and new-designed honeycomb radial rim seal with three sealing flow rate by means of three-dimensional URANS equations and SST turbulence model. The swirl velocity of ingested gas is weakened by the honeycomb and the sealing efficiency of the new-designed honeycomb radial rim seal is higher than that of the conventional one by 9-14% at the same sealing flow rate. Joshua T.M. et al. [7] numerically simulated the interaction between the main flow and the purge flow based on the DLR TRACE solver. Computations from model with different sector size resulted in no significant changes in the level of ingress. Feng Gao et al. [8] represented large-eddy simulations (LES) and unsteady Reynolds-averaged Navier-Stokes (URANS) calculations of a turbine rim seal configuration without any vanes, blades or external flows. A sector LES model showed a rather small improvement in mean pressure prediction compared to URANS models. Xingyun Jia et al. [9] solved the temperature and deformation of a turbine disc in multi-physics fields. The hot running rim seal makes cooling effectiveness in cavity decreases 2.35-6.77%, the temperature of the stator disc surface increases 16.5-62.2 K, and the thickness of the turbine platform growths 11.89-18.11%. A numerical comparison of sealing performance between conventional radial rim seal and seven different kinds of groove radial rim seal with three coolant flow rates is presented by Shuxian CHEN et al. [10] The groove rim seals can increase the sealing efficiency, and the axial groove case results in less minimum sealing flow rate than oblique groove cases. WANG Ruonan et al. [11] designed a new rim seal structure with auxiliary sealing holes compared with conventional counterpart using validated CFD methods. The results showed that additional secondary sealing flow input from auxiliary sealing holes could improve sealing efficiency in disk cavity. Seok Min Choi et al. [12] analyzed sealing efficiency of rim seal modified from an aero-engine gas turbine at various conditions Rotational Reynolds number varied from 3×10^5 to 5×10^5. A predicted correlation for sealing efficiency of rim seal was derived at various coolant mass flow rate. Ziqing ZHANG et al. [13] found that the structure of the upper part of the seal is the key factor affecting the magnitude of the loss of secondary flow caused by purge flow. Seungyeong Choi et al. [14] investigated the effect of the rotational speed of turbine blade on the unsteady hot gas ingestion under the rotational Reynolds numbers of 5.0×10^5, 1.0×10^6, 1.5×10^6. The asymmetric pressure distribution in the main flow increased as the rotational speed increased, and hot gas ingestions are likely to occur at high rotational speeds. Yang Guoqing [15] of Northwestern Polytechnical University has carried out experimental and numerical studies on the stationary cavity sealing characteristics

under the pulse detonation inflow for a single-tube reverse flow pulse detonation combustor and a single-stage turbine of a small turbine engine. The stationary cavity test rig is simplified from the 1/8 real turbine structure according to the principle of massflow conservation, and the specific simplification process can be found in Ref. [15]. Under different experimental working conditions, the pressure and temperature characteristics of each sub-cavity in the test rig are obtained. It is found that the increase of the sealing gas pressure can help to reduce the pressure pulsation inside the cavity and weaken the degree of mainflow gas ingress; and the increase of the working frequency of detonation combustor will make the temperature rise inside the cavity due to the mainflow ingestion increase accordingly.

It is clear from the above that the most of the studies have been conducted on the interaction between sealing flow and steady mainstream, except for the experiments conducted by T.Schliwka et al. [5] examined the unsteady flow characteristic around the rim seal in the condition of non-uniform mainstream provided by the Hot-Acoustic-Test Rig (HAT) wind tunnel, while their studies only focus on the pressure loss around the turbine cavity. In the research conducted by Yang Guoqing[15], the massflow-equivalent stationary cavity test rig is used, ignoring the effect of rotationally-induced ingress (RI), which may lead to a large experimental deviation.

In this paper, the numerical model validated by experimental data, the computational model designed for PDTE, as well as the simplified pulse mainstream profiles will be introduced. Based on the numerical simulations with different pressure of sealing gas, the effects of the pulse mainstream on pressure distribution and sealing efficiency is presented and clarified. Furthermore, in order to have a deeper understanding of the ingress and egress phenomenon caused by PDC, the relationship between the pressure distribution and the sealing efficiency is discussed.

2. Numerical method and validation

In this paper, the numerical method is validated based on the experiments conducted with 1 stage rim seal experimental facility at the University of Bath [16]. The detailed geometrical parameters of the experimental facility and the profiles of vane or blade can be found in Ref. [16]. The experimental facility has stationary parts and rotating parts in real work conditions. As a result, there must be a rotating domain and a stationary domain in the CFD model. As shown in fig. 1, the stationary/rotating interface is set in front of the rim seal based on the comparison between the numerical results and experimental data in Ref. [6].

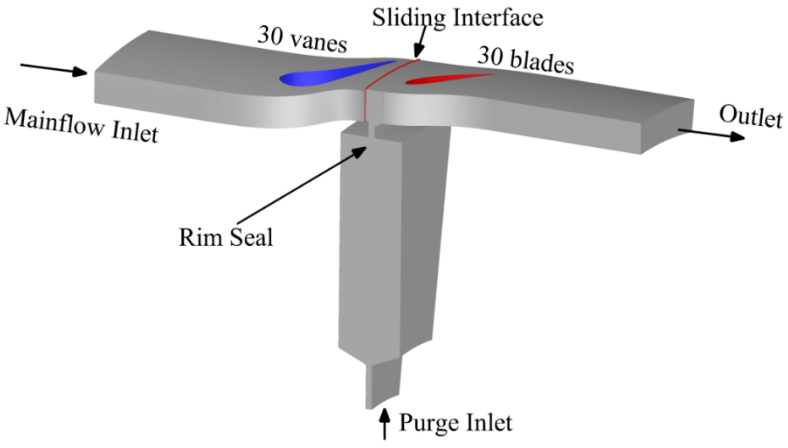

Figure 1. 11.25° sector CFD model of test rig in BATH university

The BATH experimental test rig has 32 vanes and 41 blades in a full circle. In order to reduce computational resources and meet the numerical simulation requirement, the computational model is simplified to 32 vanes and 32 blades using the Domain Scaling method[17]. The computation domain for validation incorporated one vane, one blade and a wheel-space in a 11.25 degree sector (1/32 of the annulus) is shown in fig. 1.

Parts of the boundary conditions of the computation domain are also shown in fig. 1. Periodicity is imposed at the sector model's circumferential boundaries, and the length of blade passage is much longer than axial chord of blade for ensuring that no reverse flow occurs at the outlet. According to the real experimental conditions, the boundary condition of mass flow rate is applied in the inlets of main flow path and sealing flow path. The surfaces of the wall use the adiabatic and non-slip boundary condition, only the hub and cavity walls of rotating disc have a rotating speed of zero relative to rotary disc. The outlet is set to the pressure boundary condition.

The computational grids of vane passage and blade passage are generated using ANSYS TurboGrid (version 19.2), while the computational grids of cavity is generated by ANSYS ICEM (version 19.2) using a multi-block structural method. In order to meet the precision requirements of the SST $k-\omega$ turbulence model used in the simulations, the meshes at the wall of the entire computational domain are refined. The thickness of the first layer near wall is 0.005 mm and the maximum y+ value is under 1. The entire number of meshes in the computational domain for validation is 2.39 million. ANSYS FLUENT(version 19.2), a commercial CFD code based on the finite element method, was used as solver for the numerical simulations below. The SMM model is used in the unsteady simulations, which could consider the instant vane-blade relative positions during rotating. Furthermore, the URANS method and the SST $k-\omega$ turbulence model are used. The unsteady computations require steady-state solutions for initialization, and the steady-state computations use MRF model instead of SMM model.

The concentration of trace gas is usually used to evaluate the sealing efficiency in the experimental researches.3 In numerical researches, an additional scalar variable is always used to calculate the sealing efficiency [1,2,7,8]. As a result, a User-Defined Scalar (UDS) is adopted to calculate the sealing efficiency in the numerical simulations of current paper. The conservation equation of the diffusion processes and turbulent transportation for the UDS is represented as follows:

$$\frac{\partial(\rho\varphi)}{\partial t}+\nabla(\rho U\varphi)=\nabla\left(\left(\rho D_{\varphi}+\frac{\mu_t}{Sc_t}\right)\nabla\varphi\right)\#(1)$$

Where U is the fluid velocity, ρ is the density, φ is the conserved quantity per unit mass, D_{φ} is the kinetic diffusion coefficient for the UDS, Sc_t and μ_t is the turbulence Schmidt number and the turbulence viscosity, respectively. The kinetic diffusion coefficient is set to a constant value of $1.6\times10^{-5}m^2/s$ referring to Ref. [18]. The values of the UDS are set to 0 and 1 at the mainstream inlet and the sealing flow inlet, respectively. The UDS will be 0 if turbine disc cavity is fully ingested by mainstream gas, on the contrast, it will be 1 if turbine disc cavity is completely sealed.

WANG Ruonan *et al.* [19] has carried out a time-step independency study based on the computational domain for validation, and the result shows that the time-step should be set to $1.5625\times10^{-5}s$ for rotational speed is 3000 rpm, corresponding to 40 time-steps per blade passing period.

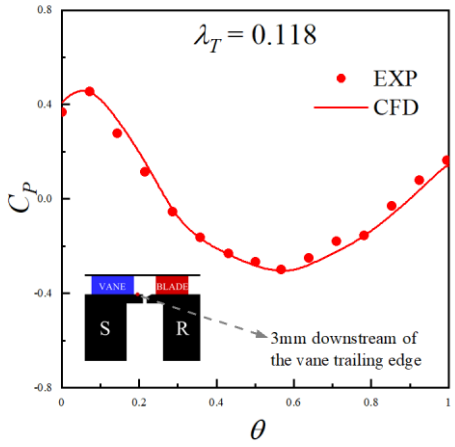

Figure 2. The distribution of C_P

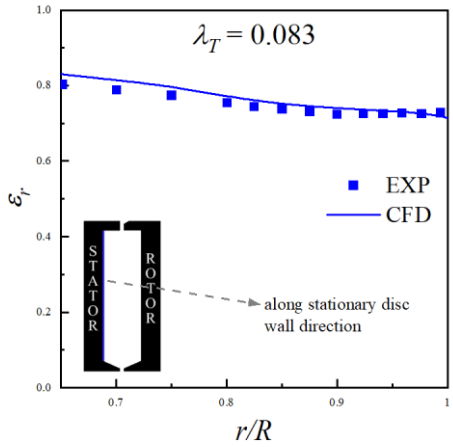

Figure 3. The distribution of ε_r

Fig. 2 shows the static pressure coefficient distribution along the circumferential direction at the vane hub. The pressure distribution simulated by unsteady computations are in good agreement with the data measured from experiments, which proved the pressure field can be well predicted using the numerical approaches above. As shown in fig. 3, also, the experimental results and numerical results of the sealing efficiency along the radial direction at the stationary disc wall are compared. It presents that the numerical simulated sealing efficiency are in good agreement with the measured experimental data in working condition of $\lambda_T = 0.083$. Thus, the validity of the numerical method of the UDS for the sealing efficiency inside the cavity is demonstrated.

3. Geometric model and computational mesh

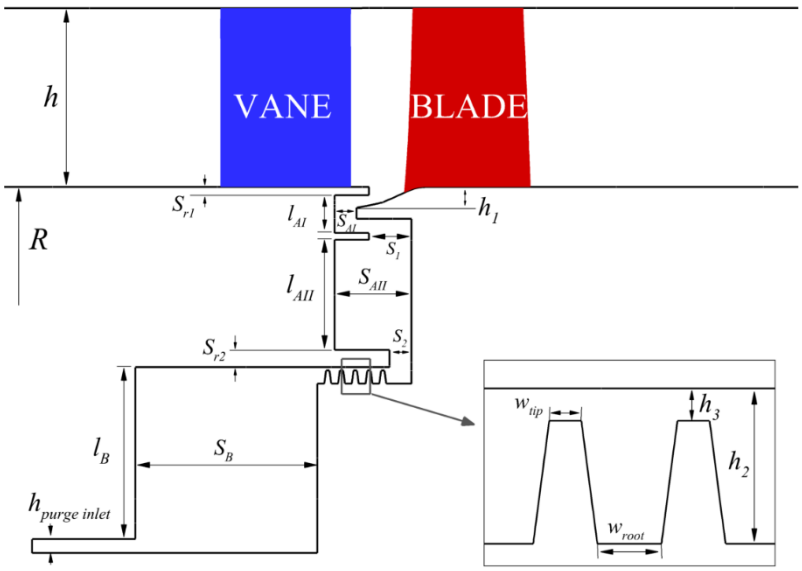

Figure 4. Structure of cavity in the meridional plane

The structure and geometric configuration of turbine stage and cavity under the pulse detonation mainstream is shown in fig. 4, and the corresponding geometric parameters are listed in tab. 1. The structure of cavity is designed complex for preventing the ingestion of pulse detonation inflow. The cavity is divided into three sub-cavities for analyze convenient, respectively, cavity AI, cavity AII and

cavity B. The vane and blade height both are 26 mm; the outer radius of cavity is 92 mm; the axial clearances are 3 mm, 11 mm and 26 mm, respectively for cavity AI, cavity AII and cavity B.

Table 1. Geometric parameters

Parameter	Value/mm	Parameter	Value/mm
h	26	S_{AI}	3
h_1	3	S_{AII}	11
h_2	2.5	S_B	26
h_3	1	S_1	6
$h_{purge\ inlet}$	2	S_2	3
R	92	S_{r1}	1
l_{AI}	5	S_{r2}	2.5
l_{AII}	16	w_{tip}	0.5
l_B	25	w_{root}	1

Although the turbine component designed for PDTE has 30 vanes and 39 blades in a full circle, the numerical simulation simplified it to 30 vanes and 30 blades in the same way validated above. As a result, the CFD domain shown in fig. 5 contained one vane, one blade and a wheel-space in a 12 degree sector (1/30 of the annulus).

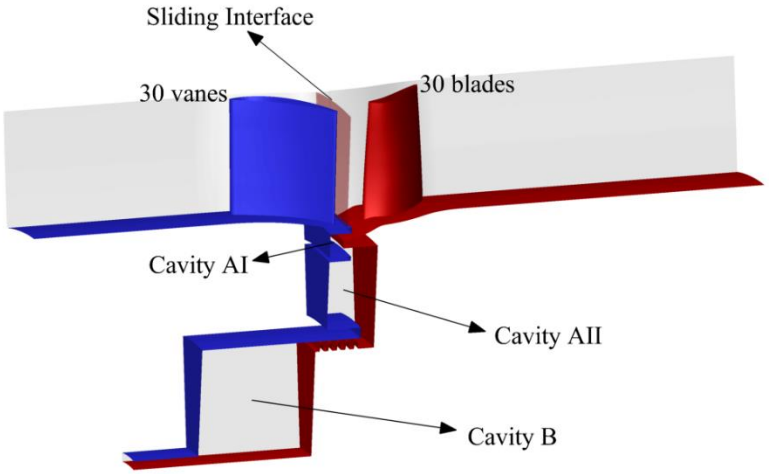

Figure 5. Computational domain of rim seal

Fig. 6 illustrates the multiblock structured grids of the 12 degree sector model. The grids generation method validated above is utilized. The 12 degree sector model contained 5.13 million cells in total. The sealing efficiency and flow field of the turbine stage and cavity under pulse detonation inflow are computed through ANSYS-FLUENT (version 19.2) solver using three-dimensional URANS model and SST $k-\omega$ turbulence model combined with an UDS method. The rotating speed designed for rotating disc is 25000 rpm. The time-step in unsteady simulation is set to 2×10^{-6} s, corresponding to 40 time-steps per blade passing period.

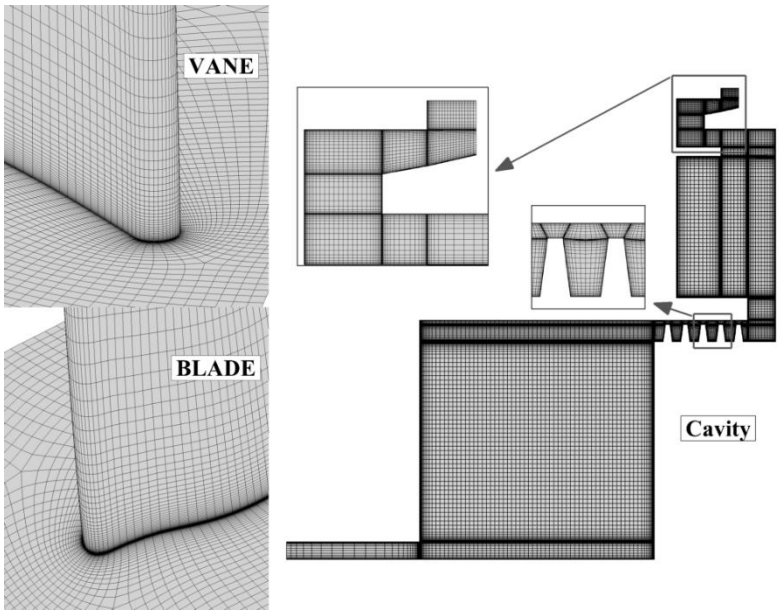

Figure 6. Computational grids

Base on the pressure profiles presented in several prior investigations [20-22] for PDC, simplified total pressure and total temperature profiles in the inlet of mainstream are generated using an exponential decay with respective specified time constant presented in Eq. (2), (3).

$$P_{Total} = P_{Tbase}\left(1 + A_P exp\left[-\frac{t}{\tau}\right]\right) \#(2)$$

$$T_{Total} = T_{Tbase}\left(1 + A_T exp\left[-\frac{t}{\tau}\right]\right) \#(3)$$

The frequency of pulse detonation combustion was set to 20 Hz, that is, the period that a pulse detonation combustion cycle needed is 0.05 s. The nominal time decay constant (τ) is set to 0.005 s, 10% of a PDC cycle period. The P_{Tbase} and T_{Tbase} respectively are the total pressure and total temperature of the mixture with which the combustion chamber filled. The peak values for total pressure and total temperature were equivalent to the results calculated by the Chapman-Jouquet Detonation module in NASA CEA using a stoichiometric fuel-oxidant mixture. Moreover, in order to consider the the DDT process that occurs in real pulse detonation combustion, the time required for one revolution of the turbine is used to represent the DDT time before each aerodynamic parameter fluatuates.

The simplification above allows for a clean investigation of the impact of the unsteady, pulse mainstream on the cavity and turbine stage. The detailed boundary conditions of cases studied and numerical approaches for current study are summarized in tab. 2.

Table 2. Boundary conditions and numerical methods

Mainstream inlet	P_{total} T_{total}	Turbulence model	SST $k-\omega$
Cavity inlet	0.5 MPa; 1 MPa; 1.5 MPa	Periodic interface	Rotational periodicity
Outlet pressure	101325 Pa	Relative motion model (steady)	MRF
Rotating speed	25000 rpm	Relative motion model (unsteady)	SMM

Fluid	Air (ideal gas)	Wall properties	Adiabatic, smooth

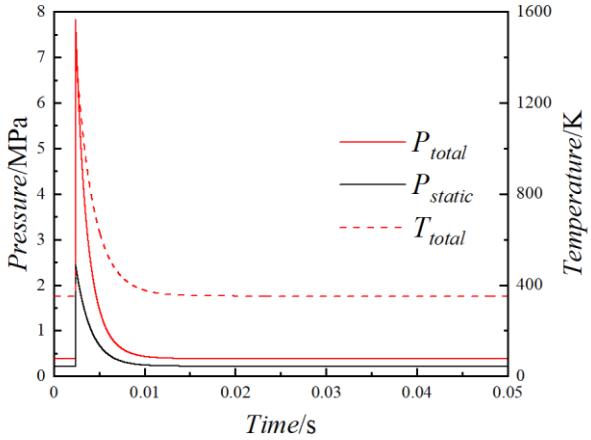

Figure 7. Simplified profiles of PDC inlet boundary condition

Fig. 7 shows the instantaneous total pressure, static pressure and total temperature applied to the inlet of mainstream path. The pressure and temperature profiles are linearly interpolated to a csv format for input into solver as the transient quantities at mainstream passage inlet.

An appropriate number of grids should be selected to reduce the computational resources with little effect on the accuracy of the numerical simulation. The average sealing efficiency at the stationary disc wall in cavity AII was calculated with 2.25 million, 5.13 million and 7.56 million grids, respectively. tab. 3 shows the values of sealing efficiency with different number of computational grids, from which the sealing efficiency is hardly changed when the grid number is greater than 5.13 million. Consequently, the computational domain with 5.13 million grids is adopted in the following simulations.

Table 3. Grid Independency

Number of Grids (million)	Sealing efficiency	Relative error
2.25	0.532	
5.13	0.571	7.33%
7.56	0.575	0.7%

4. Results and discussions

30 vane passages will be passed by one blade as long as the rotating disk rotates one revolution, that is, the number of blade passing periods (N) corresponding to one revolution is 30. The vane-blade relative positions will change periodically when the blade passes the vane passages. fig. 8 shows four classic vane-blade relative positions, $L1$, $L2$, $L3$ and $L4$, extracted from one blade passing period. The leading edges of the blades at $L1$ and $L4$ are close to the trailing edges of the vane, and the leading edges of blade at $L2$ and $L3$ are far away from the trailing edges of the vanes. The red solid line located in 1 mm upstream of cavity outlet indicates the range of normalized angle between vanes. The time-averaged static pressure coefficient ($\overline{C_P}$) is defined as:

$$\overline{C_P} = \frac{\bar{P} - P_{ref}}{0.5\rho\Omega^2 R^2} \#(4)$$

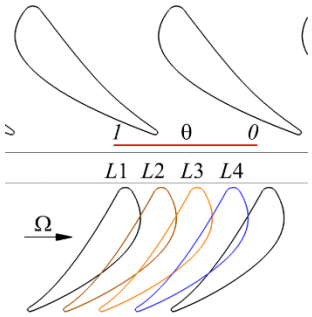

Figure 8. Four Classic vane-blade relative positions

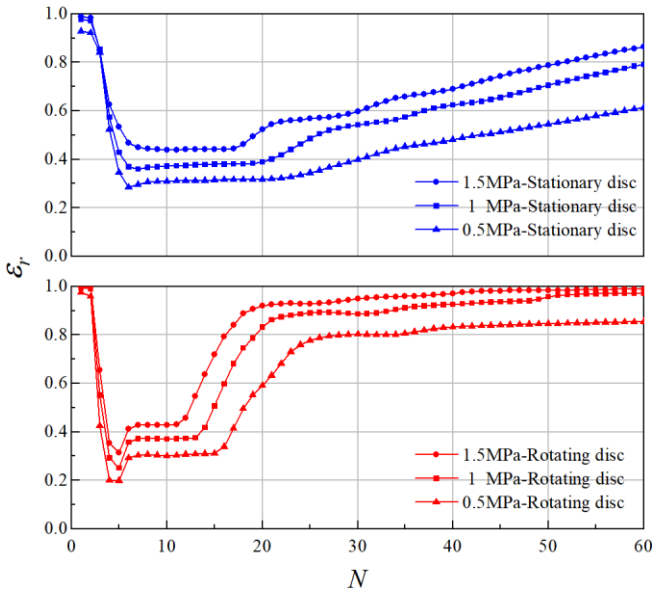

Figure 9. The evolution of time-averaged Sealing efficiency

The vertical axis in fig. 9 represents the surface-averaged sealing efficiency in cavity AII, and the horizontal axis is the number of blade passing periods. The sealing efficiency in cavity AII under the influence of the PDC inflow will go through a process of sudden drop and gradual recovery. In this paper, the process is divided into three sub-stages for further discussion, respectively, " the decline stage", " the plateau stage " and " the recovery stage ".

When the sealing gas pressure is 1 MPa. The instanteous sealing efficiency contours on five different meridional planes at the inner of cavity are shown in fig. 10. We can easily find that the flow direction at the cavity outlet is consistent at different circumferential positions, which may be caused by the excessive pressure difference between the cavity inside and outside due to the detonation peak pressure. Considering the similarity of the flow direction along the circumferential direction, the streamlines plotted on the enlarged iiith meridional plane are also shown in fig. 10.

The flow field in the computational domain won't be affected by the PDC inflow until N=0. $\bar{\varepsilon_r}$ of the stationary disc wall and rotating disc wall both are equal to 1, indicating the cavity is fully sealed at N=0. The PDC gas flows into the mainstream passage at $N1L1$. $\bar{\varepsilon_r}$ of the rotating disc wall and stationary disc wall respectively decreases to 0.97 and 0.99 at N=1, indicating the sealing efficiency of the disc cavity begins to be affected by the PDC inflow at N=1, as a result, "the decline stage" begins at N=1.

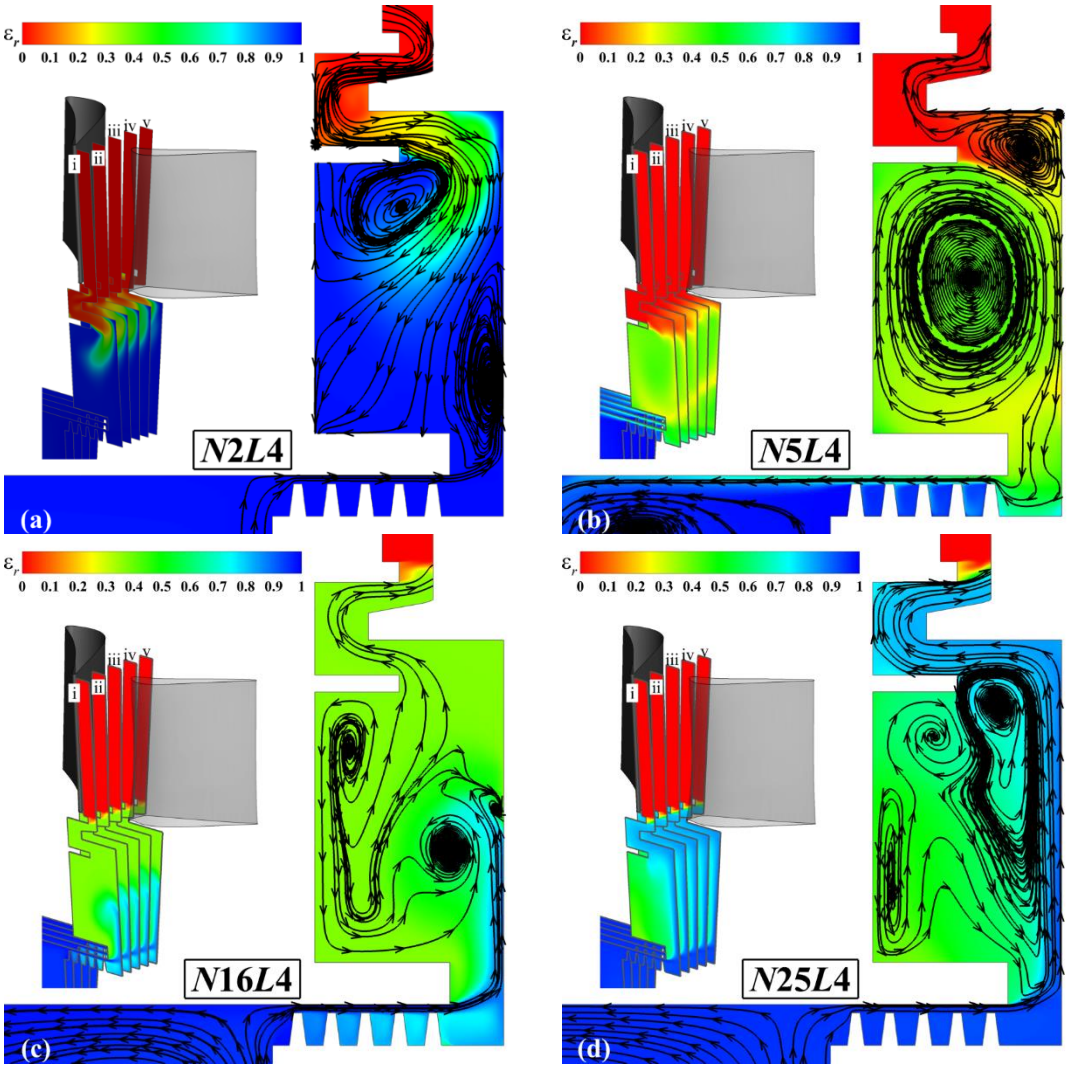

Figure 10. Instant sealing efficiency contours and the flow structure

Fig. 10(a) shows the flow structure inside the cavity at *N*2*L*4, and the ingestion of mainstream gas can be found. The PDC inflow is flowing through the cavity outlet at *N*=2. The mainstream gas ingress into the cavity AII via the cavity AI. The ingestion gas firstly arrives at the high radius positions of the rotating disc wall in cavity AII, at where the sealing efficiency decreases. Then the majority of the ingestion gas turns direction flows towards the stationary disc wall of cavity AII, while the other flows towards cavity B along the rotating disc wall direction. A vortex flow structure composed of the gas egress from cavity B and the gas ingress from cavity AII can be clearly seen at the intersection between cavity AII and cavity B. $\overline{\varepsilon_r}$ in the stationary disc wall along the radial direction is smaller than that in the rotating disc wall at *N*=1. $\overline{\varepsilon_r}$ decreases slightly at the high radius regions of the rotating disc wall at *N*=2 due to the ingress gas, while $\overline{\varepsilon_r}$ in the stationary disc wall remains the distribution at *N*=1. At *N*=3 and *N*=4, significant changes of the $\overline{\varepsilon_r}$ distributions can be found, $\overline{\varepsilon_r}$ along the stationary and rotating disc wall both decreases, and $\overline{\varepsilon_r}$ in the rotating disc wall is smaller than that of stationary disc wall along the radial direction.

Fig. 10(b) shows the flow structure inside the cavity at *N*5*L*4. A vortex flow structure with small size appears at the outlet of the cavity AI, at where the local gas egress into the mainstream, which might be drived by the pressure difference between the high-pressure ingestion gas and the decreased low-pressure mainstream gas. Another vortex flow structure fully filled the whole room of cavity AII

is generated at *N*=5, which makes the distribution of the sealing efficiency field in the cavity AII more even. $\overline{\varepsilon_r}$ increases to 0.43 for the stationary disc wall, $\overline{\varepsilon_r}$ increases to 0.25 for the rotating disc wall. The area along the radial direction with the same value of $\overline{\varepsilon_r}$ in the stationary disc wall and rotating disc wall begins to increase. Meanwhile, a small portion of the ingestion gas ingress into the cavity B through the labyrinth seal. The value of $\overline{\varepsilon_r}$ in stationary disc wall and rotating disc wall are both 0.37 at *N*=6. Only at the positions with high radius or low radius $\overline{\varepsilon_r}$ in stationary disc wall is a little higher than that in rotating disc wall.

The sealing efficiency field in cavity AII distributes more homogeneous under the influence of the vortex flow structure. In "the plateau stage", $\overline{\varepsilon_r}$ of stationary and rotating disc walls always maintains at the same low value as fig.9 illustrates.

"The recovery stage" is the period that the sealing efficiency in the cavity recovers to the level without the effect of the PDC inflow. The start time in "the recovery stage" of the stationary and rotating disc wall are *N*=20 and *N*=13, respectively. At *N*=13, $\overline{\varepsilon_r}$ along the radial direction of the stationary and rotating disc wall are both equal to 0.37, as fig.9 shows. fig. 10(c) shows the flow structure inside the cavity at *N*16*L*4. The sealing gas in cavity B egresses to the low radius in the cavity AII via the labyrinth seal, resulting in $\overline{\varepsilon_r}$ in the low radius of the rotating disc wall increases to 0.85. The sealing efficiency in the rotating disc wall will increase from low radius to high radius. However, the sealing efficiency in the stationary disc wall maintains with value 0.37 until *N*=20. $\overline{\varepsilon_r}$ of the rotating disc wall recovers to 0.9 at *N*=22, and it evenly distributes along the radial direction. $\overline{\varepsilon_r}$ of the stationary disc slowly increases from high radius to low radius along the radial direction, such as *N*=22, *N*=25, *N*=28 shown in fig. 9.

fig. 10(d) shows the flow structure inside the cavity at *N*25*L*4. At *N*=25, large amounts of the sealing gas egress into the mainstream path along the rotating disc wall. The sealing efficiency near the rotating disc wall increases to 0.9, and for the stationary disc wall, the sealing efficiency with high radius increases to 0.52.

For "the recovery stage" with the sealing gas pressure is 0.5MPa, $\overline{\varepsilon_r}$ of the stationary and rotating disc walls increase to 0.6 respectively need 38 and 5 blade passing periods. For the sealing gas pressure is 1MPa, the number of blade passing periods needed are 17 and 3, respectively. For the sealing gas pressure is 1.5MPa, the number of blade passing periods needed are 12 and 2, respectively. Due to the increase of the sealing gas pressure, the sealing efficiency of the stationary and rotating disc walls increases, while the period of "the plateau stage" decreases. $\overline{\varepsilon_r}$ within "the plateau stage " increases from 0.31 to 0.42 with the sealing gas pressure grows from 0.5 MPa to 1.5 MPa, and the number of blade passing periods contained in "the plateau stage" reduce from 16 to 11, 10 to 6, respectively for stationary disc wall and rotating disc wall. The period of "the recovery stage" in the stationary and rotating disc walls both decreases with the growth of the sealing gas pressure, however, for the same sealing inflow pressure, the period of "the recovery stage" in the stationary disc wall always longer than that in the rotating disc wall.

Fig. 11 shows the annulus distribution of pressure and sealing efficiency with different radii as the sealing gas pressure is 1 MPa, respectively, at *N*=0, *N*=3, *N*=10 and *N*=27. *N*=0 represents the period with no effect of the PDC inflow, and *N*=3, *N*=10, *N*=27 individually represent the periods of "the decline stage", " the plateau stage" and "the recovery stage".

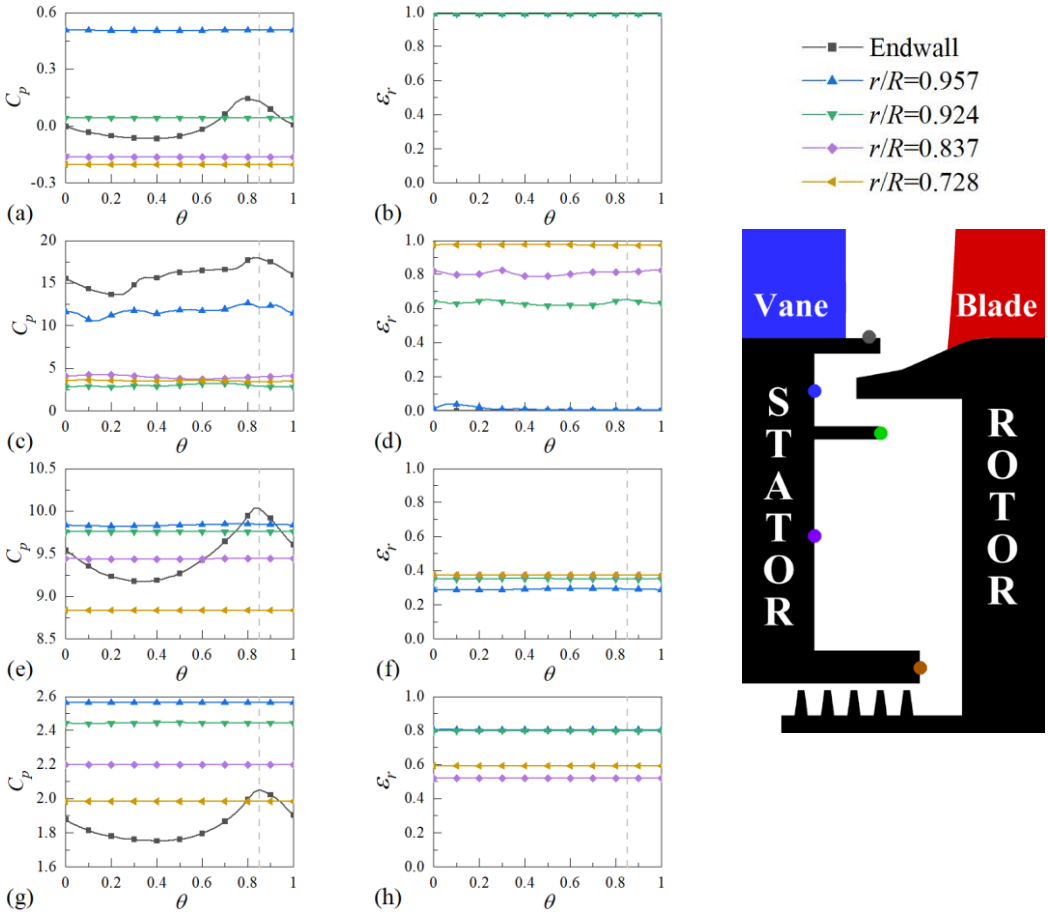

Figure 11. Time-averaged C_P and Sealing efficiency distribution in the annulus

At *N*=0, in the 1mm upstream of the cavity outlet, the maximum and minimum values for $\overline{C_P}$ are 0.15 and -0.1, respectively. The area of pressure peak at the upstream of the cavity outlet is 0.75-0.85, corresponding to the region around the vane trailing edge, and the area of pressure trough is located in the position of vane passage. This kind of pressure distribution occurs because the vane passage accelerates the speed of main flow. This tendency of distribution has no significant difference even if the pressure of mainstream is highly unsteady caused by the PDC inflow. As shown in fig. 11(a),(c),(e),(g), the pressure peak in the position of vane trailing edge can also be found at *N*=3, *N*=10 and *N*=27, however, the exact values of pressure peak and pressure trough at different instant are changed.

Fig. 11(a) shows that the pressure distributions at *r/R*=0.957 is higher than that of the end wall at *N*=0. The sealing gas egresses to the mainstream passage in the whole annulus due to the pressure difference. As a result, the sealing efficiency at every location inside the cavity is 1, as shown in fig. 10(b), which indicates the cavity is completely sealed when the mainstream is not affected by the PDC inflow.

Fig. 11(c) shows the pressure distributions at *N*=3. $\overline{C_P}$ at endwall increases to 15 under the influence of the PDC inflow, which is larger than that of other radial locations inside the cavity. The mainstream gas ingresses into cavity from high radius to low radius, resulting in $\overline{C_P}$ at *r/R*=0.957 increases to about 11, and the pressure at *r/R*=0.924, 0.817 and 0.728 region both increases slightly. The sealing efficiency decreases to 0 at *r/R*=0.957, which indicates this location has been fully

ingressed. Furthermore, the sealing efficiency at the other radial positions decreases with the increased radius, as shown in fig. 11(d).

It can be clearly seen from fig. 11(e) that the pressure distributions inside the cavity increases with the increased radius at *N*=10 and $\overline{C_P}$ at endwall decreases to 9-10, and C_P of the endwall is lower than that inside the cavity in most circumferential areas. The sealing efficiency at *r/R*=0.924, 0.817 and 0.728 inside the cavity AII are both 0.4, as shown in fig. 11(f). This phenomenon is consistent with conclusion above that the vortex flow structure inside the cavity makes the sealing efficiency distributes homogeneous.

The pressure distributions inside the cavity and at endwall decreases at *N*=27 as shown in fig. 11(g). $\overline{C_P}$ at endwall decreases to 1.9-2.1. The pressure inside the cavity increases as the radius increases, and the pressure inside the cavity is larger than that at endwall in most areas in the annulus, thus the egress effect might occur. The egress of sealing flow makes the sealing efficiency inside the cavity increases, as shown in fig. 10(h). However, the sealing efficiency at *r/R*=0.837 and *r/R*=0.728 are 0.5 and 0.6, respectively, which are both lower than the value at the higher radius positions. The sealing gas inside the cavity B straightly egress to the cavity AI along the rotating disc wall of cavity AII, resulting in the sealing efficiency in cavity AII increases slowlier than cavity AI.

In "the decline stage", the pressure magnitude at the upsteam of the rim seal outlet increases due to the PDC inflow, resulting in the mainstream gas ingress into the cavity, and the sealing efficiency inside the cavity begins to decreases. In "the plateau stage", the pressure at the upsteam of the cavity outlet is almost equivalent to the pressure inside cavity, the flow structure inside the cavity is almost steady, so that the sealing efficiency basically doesn't change. In "the recovery stage", the pressure at the upsteam of the cavity outlet decreases to the value lower than that inside the cavity, the sealing gas starts to egress into the mainstream, resulting in the sealing efficiency slowly recovers to 1.

5. Conclusion

The current research presents the unsteady processes of the turbine mainstream gas / sealing gas interaction forced by the pulse detonation combustion. A detailed understanding of the interaction between the PDC inflow and the sealing gas is discussed in this paper, and the results of the research are as following concluding remarks:

（1）The flow characteristics and sealing efficiency are investigated using 3D Unsteady Reynolds-Averaged Navier-Stokes (URANS) equations and SST $k-\omega$ turbulent model. The numerical method is firstly validated through experimental data of BATH university. Refer to the several prior investigations for PDC, the PDC inflow boundary condition applied to the inlet of mainstream passage is simplified based on simple exponential decay formulas.

(2)By scrutinizing the instantaneous flow field and sealing efficiency distribution, obvious ingress and egress processes can be identified around the circumference in the outlet region of the cavity due to the PDC inflow. This paper divides the interaction process into three sub-stages based on the change laws of sealing efficiency and the flow structures inside the cavity, respectively, " the decline stage", " the plateau stage " and " the recovery stage ". It is believed that the difference between the static pressure at endwall and that inside the cavity drives the ingress and egress effect.

(3)From the numerical simulation results. The sealing efficiency inside the cavity will increase as the sealing gas pressure grows, and the period of " the plateau stage" and " the recovery stage" will

be decreased, resulting in an improvement in the ability of turbine cavity to resist the ingress of PDC inflow.

Acknowledgment

This work was Supported by China Space Foundation Aerospace Propulsion Public Welfare Special Fund and the Natural Science Foundation of Shaanxi Province of China through Grant No. (2024JC-YBMS-356).

Nomenclature

C_P - static pressure coefficient (= $(P - P_{ref})/0.5\rho\Omega^2R^2$), [–]
$L1$, $L2$, $L3$, $L4$ - the vane-blade relative positions, [–]
N - Number of blade passing periods, [–]
Ni - Number of blade passing periods = i, [–]
$\bar{P}$ - time-averaged static pressure, [Pa]
$P_{coolant}$ - total pressure at cavity inlet, [MPa]
P_{ref} - time-averaged static pressure in the annulus without the effect of PDC inflow, [Pa]
r - radius, [m]
R - outer radius of cavity, [m]

Greek Letters

ε_r - sealing efficiency, [–]
λ_T - Turbulent flow parameter, [–]
θ - normalized angle between vanes, [–]
ρ – density, [kgm-3]
Ω - angular speed of rotating disc, [rads-1]

Subscripts

max - maximum value in the annulus
min - minimum value in the annulus

Abbreviations and acronyms

AI - cavity AI
AII - cavity AII
B - cavity B
BPP - Blade Passing Period
MRF - Multiple moving Reference Frame
R - Rotating disc
static - static quantity
S - Stationary disc
SMM - Sliding Mesh Model
UDS - User-Defined Scalar

References

[1] Heiser, W. H., Pratt, D. T., Thermodynamic cycle analysis of pulse detonation engines, *Journal of propulsion and power*, *18* (2002), 1, pp. 68-76

[2] Roy, R. P., *et al.*, The flow field and main gas ingestion in a rotor-stator cavity, *Proceedings*, Turbo Expo: Power for Land, Sea, and Air, 2007, 47934: 1189-1198

[3] Zhou, D. W., *et al.*, Main gas ingestion in a turbine stage for three rim cavity configurations, 2011

[4] Teuber, R., *et al.*, Computational extrapolation of turbine sealing efficiency from test rig to engine conditions, *Proceedings of the Institution of Mechanical Engineers*, *227* (2013), 2, pp. 167-178

[5] Schliwka, T., *et al.*, Interaction of main flow and sealing air across a turbine cavity under unsteady conditions, *Proceedings*, ISABE-22th International Symposium on Air Breathing Engines, Phoenix, Arizona, USA, 2015

[6] Li, J., *et al.*, Numerical investigations on the sealing efficiency of turbine honeycomb radial rim seal, *Journal of Engineering for Gas Turbines and Power*, *138* (2016), 10, 102601

[7] Horwood, J. T. M., *et al.*, Unsteady computation of ingress through turbine rim seals, *Proceedings*, Turbo Expo: Power for Land, Sea, and Air, American Society of Mechanical Engineers, 2018, 51098: V05BT15A012

[8] Gao, F., *et al.*, Advanced numerical simulation of turbine rim seal flows and consideration for RANS turbulence modelling, *Proceedings*, Turbo Expo: Power for Land, Sea, and Air, American Society of Mechanical Engineers, 2018, 51098: V05BT15A005

[9] Jia, X., *et al.*, Numerical investigation on the effect of hot running rim seal clearance on hot gas ingestion into rotor-stator system, *Applied Thermal Engineering*, *152* (2019), pp. 79-91

[10] Chen, S., *et al.*, Numerical Investigations on the Sealing efficiency of Turbine Groove Radial Rim Seal, *Proceedings*, Turbo Expo: Power for Land, Sea, and Air. American Society of Mechanical Engineers, 2019, 58653: V05BT15A002

[11] Wang, R., *et al.*, Influence of secondary sealing flow on performance of turbine axial rim seals, *Journal of Thermal Science*, *29* (2020), pp. 840-851

[12] Choi, S. M., *et al.*, Effect of various coolant mass flow rates on sealing efficiency of turbine blade rim seal at first stage gas turbine experimental facility, *Energies*, *13* (2020), 16, 4105

[13] Zhang, Z., *et al.*, Flow mechanism between purge flow and mainstream in different turbine rim seal configurations, *Chinese Journal of Aeronautics*, *33* (2020), 8, pp. 2162-2175

[14] Choi, S., *et al.*, Unsteady hot gas ingestion through the double rim-seals of an axial gas turbine, *International Journal of Mechanical Sciences*, *207* (2021), 106664

[15] Yang, G., Numerical Simulation and Experimental Study of Turbine Disc Sealing under Pulse Detonation Incoming Flow, M. Sc. thesis, Northwestern Polytechnical University, 2023

[16] Sangan, C. M., Measurement of ingress through gas turbine rim seals, Ph. D. thesis, University of Bath, 2011

[17] Rai, M. M., Three-dimensional Navier-Stokes simulations of turbine rotor-stator interaction. Part I-Methodology, *Journal of Propulsion and Power*, *5* (1989), 3, pp. 305-311

[18]Boutet-Blais, G., *et al.*, Passive tracer validity for cooling effectiveness through flow computation in a turbine rim seal environment, *Proceedings*, Turbo Expo: Power for Land, Sea, and Air. 2011, 54655: 821-831

[19]Wang, R., Investigation on the unsteady mechanisms of rim seal flow and the control methods of hot gas ingestion, M. Sc. thesis, Chinese Academy of Sciences, 2020

[20]Wang, L., *et al.*, Experimental and Numerical Study on working characteristics of U-shaped pulse detonation, *Proceedings*,11th 2019 Asia Pacific International Symposium on Aerospace Technology, Gold Coast, Australia, 2019: 2354-2362

[21]Lu, J., *et al.*, Experimental Investigation on the Interactions Between a Two-phase Multi-tube Pulse Detonation Combustor and a Centrifugal Compressor, *Applied Thermal Engineering*, *113* (2017), pp. 426-434

[22]Wang, D., *et al.*, Investigation on the effect of injector modification on injector atomization and U-bend pulse detonation combustion characteristics, *Thermal Science*, 2023, Online First, https://doi.org/10.2298/TSCI230513203W

Received: 14.10.2023.
Revised: 10.12.2023.
Accepted: 03.02.2024.